



Dynamic metabolic models of CHO cell cultures through minimal sets of elementary flux modes

F. Zamorano^a, A. Vande Wouwer^{a,*}, R.M. Jungers^b, G. Bastin^b

^a Department of Automatic Control, University of Mons, Boulevard Dolez 31, 7000 Mons, Belgium

^b Centre for Systems Engineering and Applied Mechanics, Department of Mathematical Engineering, Catholic University of Louvain, 1348 Louvain-La-Neuve, Belgium

ARTICLE INFO

Article history:

Received 14 January 2012

Received in revised form 16 May 2012

Accepted 21 May 2012

Available online 12 June 2012

Keywords:

Elementary flux modes

Dynamical modeling

Metabolic networks

Underdetermined systems

Mammalian cells

ABSTRACT

The concept of Elementary Flux Modes (EFMs) has been of central importance in a number of studies involving the analysis of metabolism. In [Provost and Bastin \(2007\)](#) this concept is used to translate the metabolic networks of the different phases of CHO cell cultures into macroscopic bioreactions linking extracellular substrates to products. However, a critical issue concerns the calculation of these elementary flux vectors, as their number combinatorially increases with the size of the metabolic network. In this study, a detailed metabolic network of CHO cells is considered, where the above-mentioned combinatorial explosion makes the computation of the elementary flux modes impossible. To alleviate this problem, a methodology proposed in [Jungers et al. \(2011\)](#) is used to compute a decomposition of admissible flux vectors in a minimal number of elementary flux modes without explicitly enumerating all of them. As a result, a set of macroscopic bioreactions linking the extracellular measured species is obtained at a very low computational expense. The procedure is repeated for the several cell culture phases and a global model is built using a multi-model approach, which is able to successfully predict the evolution of experimental data.

© 2012 Elsevier B.V. All rights reserved.

1. Introduction

Macroscopic models of bioprocesses have been used in many applications, ranging from simulation to estimation, optimization and control ([Bastin and Dochain, 1990](#)). These models represent the conversion of substrates into products by a few macroscopic reactions, without taking the intracellular reaction network into consideration (black box representation).

These models can be derived using two main approaches. The first approach is essentially data-driven. Macroscopic models are derived solely from the experimental observation of the time evolution of a few extracellular components (substrates, products of interest, inhibiting compounds). Various techniques can be combined, including data analysis techniques such as principal component analysis to deduce the number of bioreactions and partial stoichiometry ([Bernard and Bastin, 2005](#)), and identification methods based on – whenever possible – decoupling techniques to estimate independently the stoichiometry and the kinetics (concept of C-identifiability) ([Chen and Bastin, 1996](#); [Hulhoven et al.,](#)

[2005](#)). In the second approach, the available prior knowledge about the metabolic network is exploited, and a macroscopic set of reactions is derived in agreement with the intracellular metabolism ([Haag et al., 2005](#)).

This is the second approach which is of interest in the present study, and particularly, the procedure devised in [Provost and Bastin \(2004\)](#) where dynamic models are derived from the concept of Elementary Flux Modes (EFMs) for a metabolic network of CHO cells under balanced growth conditions. This latter assumption stipulates that the intracellular metabolites do not accumulate in the cell, or in other words, that the intracellular processes occur much faster than those happening outside the cell. In [Provost and Bastin \(2007\)](#), this approach is further used to translate the metabolic networks of the different phases of the cell culture into macroscopic bioreactions linking extracellular substrates to products. However, a critical issue concerns the calculation of these elementary flux vectors, as their number combinatorially increases with the size of the metabolic network.

This latter point is one of the motivations behind this study, in which we consider a more detailed metabolic network of CHO cells developed by the authors in [Zamorano et al. \(2010\)](#), where the above-mentioned combinatorial explosion makes the computation of the elementary flux modes impossible. To alleviate this problem, we apply a methodology to compute a decomposition of admissible flux vectors in a minimal number of elementary flux modes without explicitly enumerating all of them, as proposed by

* Corresponding author.

E-mail addresses: francisca.zamorano@umons.ac.be (F. Zamorano), alain.vandewouwer@umons.ac.be (A. Vande Wouwer), raphael.jungers@uclouvain.be (R.M. Jungers), georges.bastin@uclouvain.be (G. Bastin).

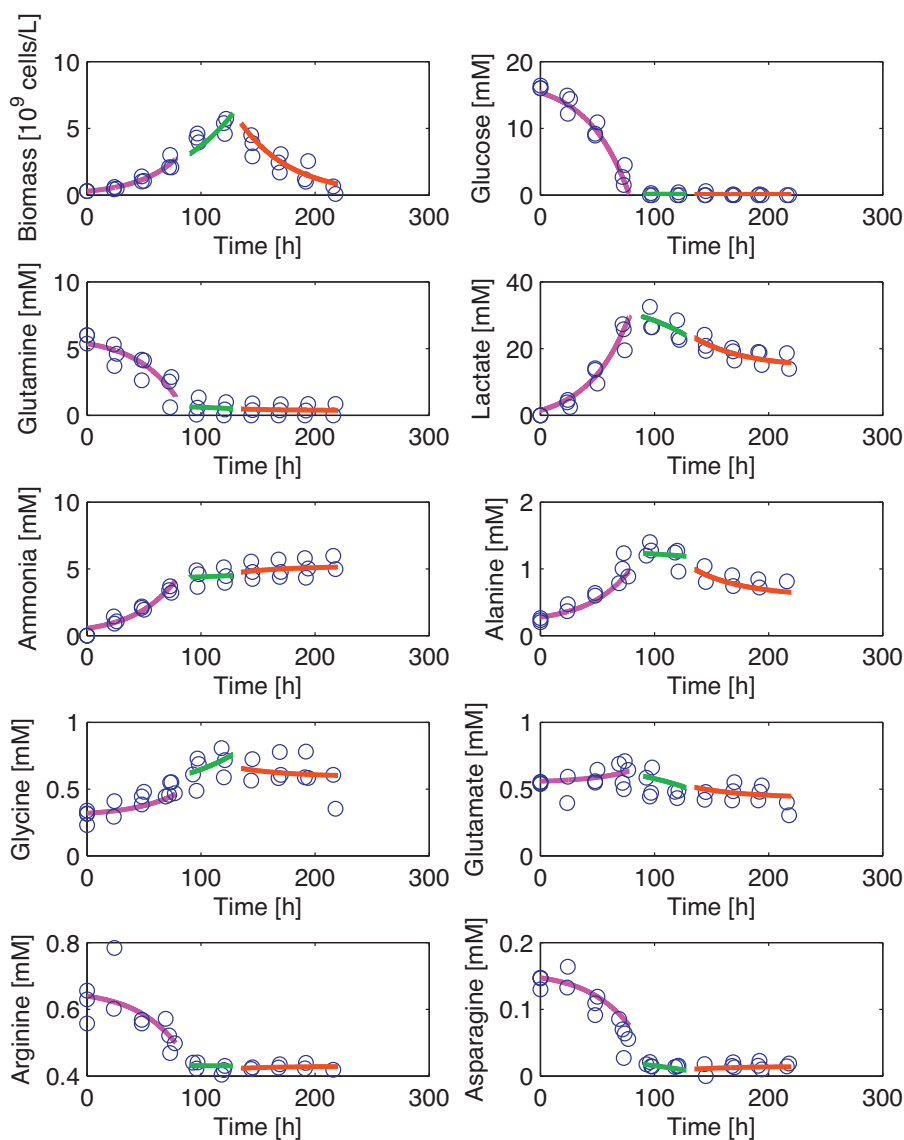


Fig. 1. Prediction of the three different models – biomass and 9 first components – magenta: growth phase model; green: transition phase model; red: death phase model.

the authors in Jungers et al. (2011). As a result, a set of macroscopic bioreactions linking the extracellular measured species is obtained at a very low computational cost. Further, the procedure is repeated for the different cell culture phases (exponential growth, transition and death) to determine local dynamic models, which can then be assembled to form a global (piecewise) model for the entire culture. The multi-model approach has already been applied successfully to describe the behavior of complex bioprocesses in other areas of applications such as wastewater treatment (Smets, 2002), or the culture of micro-algae in photo-bioreactors (Mocquet et al., 2010).

This paper is organized as follows. Section 2.1 introduces the general form of a dynamic model of batch cell cultures and the concept of Elementary Flux Modes (EFMs). The methodology for the computation of a minimal set of EFMs and the decomposition of an admissible flux distribution is presented in Section 2.2. A practical application of the methodology is presented in Section 3.1, where sets of macroscopic bioreactions are computed for each of the phases of batch cultures of CHO-320 cells. Section 3.2 discusses the construction of a piecewise dynamic model for the entire culture, based on the previous local models. Finally, Section 4 draws the main conclusions of this work.

2. Theory

2.1. Cell culture modeling

2.1.1. Dynamics of a batch culture

In general, cell cultivation in a batch process can be divided in at least three phases, according to the physiological states of the cells.

- The first phase corresponds to the exponential growth, where the concentration of the carbon source and all other substrates are in excess and there is sufficient dissolved oxygen allowing a rapid proliferation of the biomass. Lactate, alanine and ammonia are produced because of the high level of glucose and glutamine.
- The second phase is transition, where the sugar concentration decreases below a critical level and the produced lactate and alanine start to be consumed instead. There is sufficient dissolved oxygen in the medium in order to allow the oxidative pathways metabolize lactate and alanine and keep the cellular division, however in a less effective way.
- The third state corresponds to cellular death, where programmed cell death takes place upon exposure to stress encountered in the

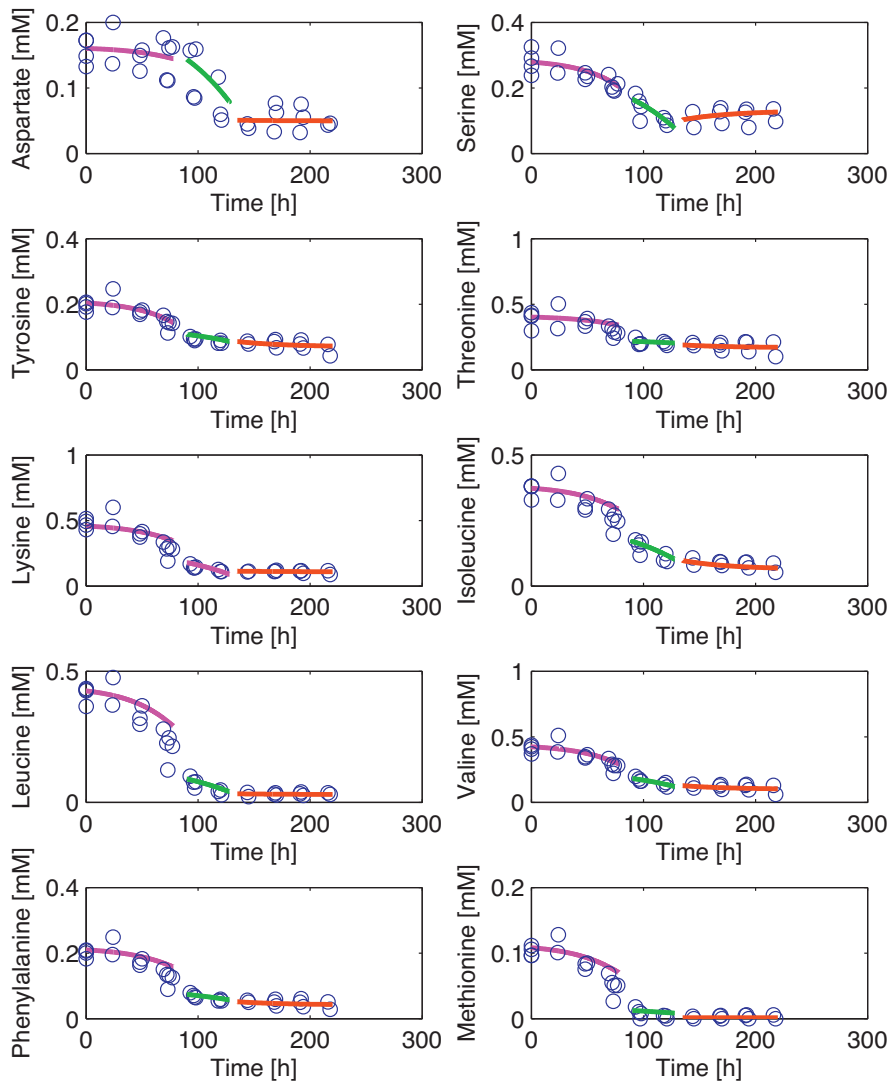


Fig. 2. Prediction of the three different models – 10 remaining components – magenta: growth phase model; green: transition phase model; red: death phase model.

bioreactor. There could be various causes for apoptosis: nutrient depletion, waste byproduct accumulation, hypoxia, mechanical agitation, etc (Arden and Betenbaugh, 2004).

The lag phase is not considered in this study as a metabolic network describing the biochemical process followed by the cells to rearrange and adapt their metabolism to the new environmental conditions would be difficult to represent and most certainly, intracellular measurements would be necessary.

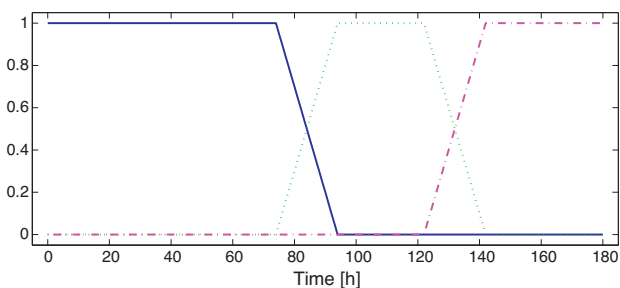


Fig. 3. Linear switching functions.

For a cell culture carried out in batch mode in a stirred tank reactor, the dynamics of substrates and products are described by:

$$\begin{aligned} \frac{d\mathbf{S}}{dt} &= -\mathbf{v}_s X(t) \\ \frac{d\mathbf{P}}{dt} &= \mathbf{v}_p X(t) \end{aligned} \tag{1}$$

where

- $X(t)$ is the biomass concentration,
- $\mathbf{S}(t)$ is the vector of substrate concentrations,
- $\mathbf{P}(t)$ is the vector of product concentrations,
- \mathbf{v}_s is the vector of specific uptake rates,
- \mathbf{v}_p is the vector of specific production rates.

Clearly, \mathbf{v}_s and \mathbf{v}_p are linear combinations of some of the (intracellular) metabolic fluxes \mathbf{v} . Thus, by defining appropriate matrices \mathbf{N}_s and \mathbf{N}_p , the stoichiometric matrices for the extracellular substrates and final products, respectively, this relation can be expressed as:

$$\begin{aligned} \mathbf{v}_s(t) &= \mathbf{N}_s \mathbf{v}(t) \\ \mathbf{v}_p(t) &= \mathbf{N}_p \mathbf{v}(t). \end{aligned} \tag{2}$$

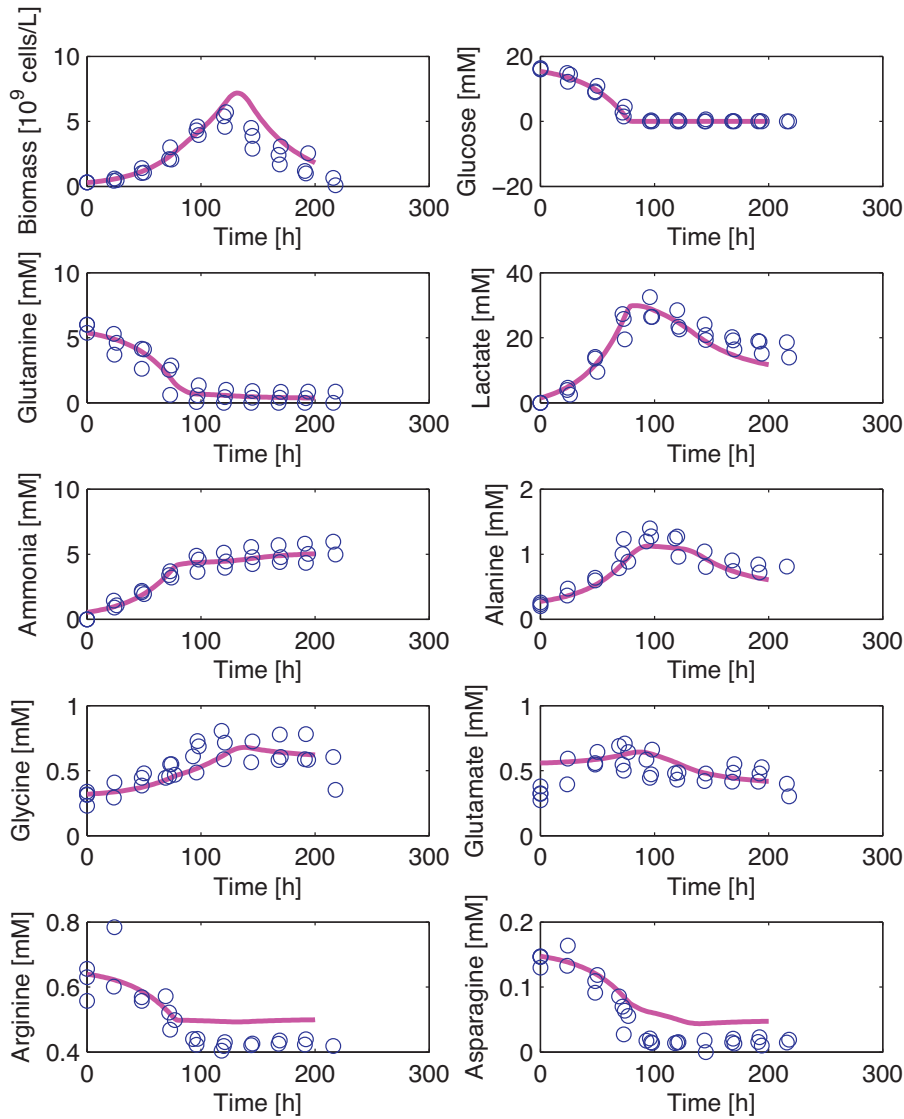


Fig. 4. Global model validation (using linear weighting functions).

2.1.2. Metabolic network and elementary flux modes

The intracellular metabolism of living cells is usually represented by a metabolic network under the form of a hypergraph encoding a set of biochemical reactions. In this hypergraph, each node represents a particular intracellular metabolite and the edges represent the metabolic reactions or fluxes.

According to the pseudo steady-state assumption of metabolic flux analysis (MFA), it is assumed that the fluxes are balanced at each internal node, i.e. intracellular metabolites do not accumulate in the cell. This means that the net sum of production and consumption fluxes, weighted by their stoichiometric coefficients, is zero for each internal metabolite of the network. This steady-state balance around the internal metabolites is expressed by the algebraic relation:

$$\mathbf{N}\mathbf{v} = \mathbf{0} \quad \mathbf{v} \geq \mathbf{0} \quad (3)$$

where $\mathbf{v} = (v_1, v_2, \dots, v_n)^T$ is the n -dimensional column vector of fluxes and $\mathbf{N} = [n_{ij}]$ is the $m \times n$ stoichiometric matrix of the metabolic network (m is the number of internal metabolites and n is the number of fluxes). More precisely, a flux v_j denotes the rate of reaction j and a non-zero n_{ij} is the stoichiometric coefficient of the metabolite i in reaction j .

For a given metabolic network, the set S of possible flux distributions is the set of vectors \mathbf{v} that satisfy the linear system (3). This set S is the pointed polyhedral cone resulting from the intersection of the kernel of \mathbf{N} with the non-negative orthant. This implies that there exists a set of elementary flux vectors \mathbf{e}_i , the extreme rays (or edges) of this polyhedral cone, such that any flux distribution \mathbf{v} can be expressed as a non-negative linear combination of them:

$$\mathbf{v} = w_1 \mathbf{e}_1 + w_2 \mathbf{e}_2 + \dots + w_q \mathbf{e}_q \quad w_i \geq 0. \quad (4)$$

The $n \times q$ non-negative matrix \mathbf{E} with column vectors \mathbf{e}_i obviously satisfies $\mathbf{N}\mathbf{E} = \mathbf{0}$ and Eq. (4) can be written in matrix form as

$$\mathbf{v} = \mathbf{E}\mathbf{w} \quad \text{with} \quad \mathbf{w} \triangleq (w_1, w_2, \dots, w_q)^T. \quad (5)$$

Thus, the elementary flux vectors are a way of representing the set of possible flux distributions. The dynamics of the concentration of each substrate and product in a batch reactor, where no exchange occurs with the outside environment, are written as follows:

$$\frac{d}{dt} \begin{pmatrix} \mathbf{S}(t) \\ \mathbf{P}(t) \end{pmatrix} = \begin{pmatrix} -\mathbf{N}_s \\ \mathbf{N}_p \end{pmatrix} \mathbf{v}X. \quad (6)$$

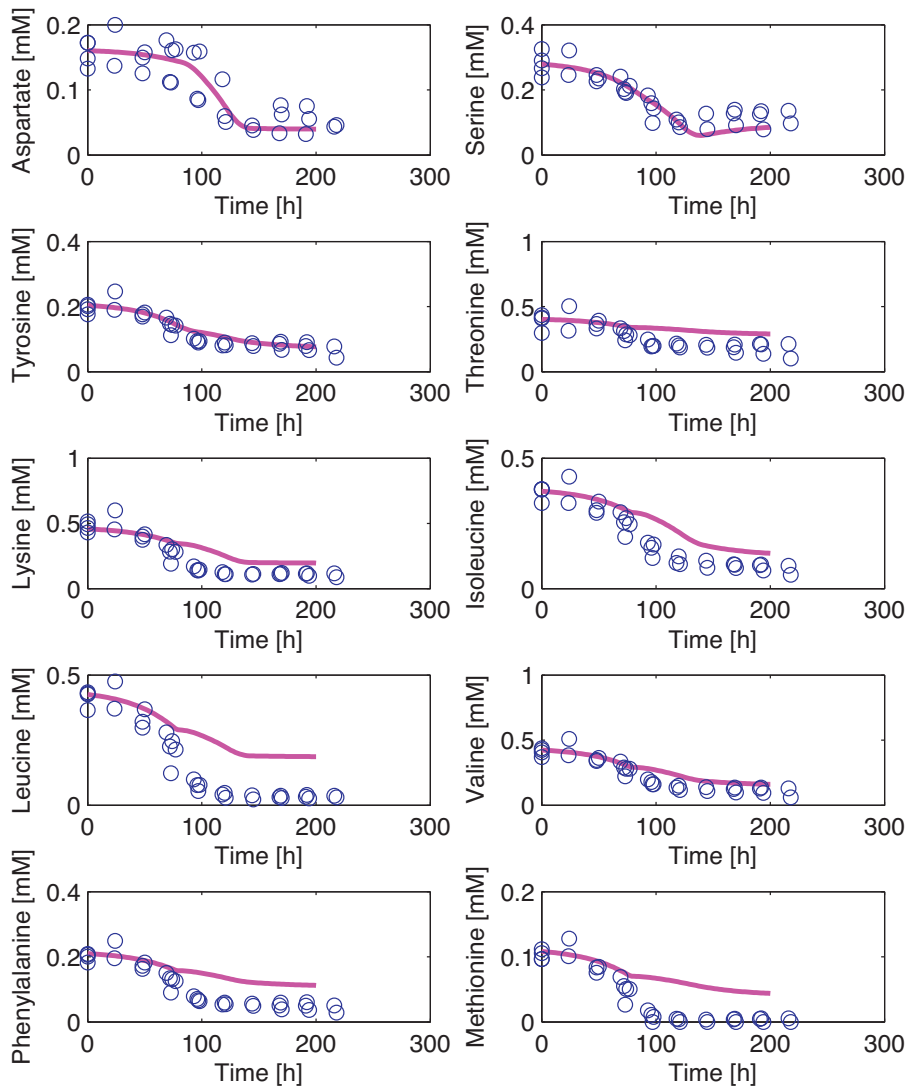


Fig. 5. Global model validation (using linear weighting functions).

From Eqs. (5) and (6), we obtain:

$$\frac{d}{dt} \begin{pmatrix} \mathbf{S}(t) \\ \mathbf{P}(t) \end{pmatrix} = \begin{pmatrix} -\mathbf{N}_s \\ \mathbf{N}_p \end{pmatrix} \mathbf{E} \mathbf{w} X. \quad (7)$$

The product of stoichiometric matrices \mathbf{N}_s and \mathbf{N}_p times the elementary flux modes matrix \mathbf{E} yields the stoichiometric matrix for a set of macroscopic reactions, linking the extracellular substrates to the final products. Let us consider that the reaction scheme of the process involves N macroscopic reactions and M extracellular species, either substrates or products, with \mathbf{K} being the $M \times N$ matrix for the stoichiometric coefficients.

$$\mathbf{K} = \begin{pmatrix} -\mathbf{N}_s \\ \mathbf{N}_p \end{pmatrix} \mathbf{E} \quad (8)$$

Then, if the vector ξ is defined as:

$$\xi = \begin{pmatrix} \mathbf{S}(t) \\ \mathbf{P}(t) \end{pmatrix}, \quad (9)$$

The dynamic model defined by the macroscopic bioreactions may be written as:

$$\frac{d\xi}{dt} = \mathbf{K} \mathbf{w}(t) X(t) = \mathbf{K} \varphi(\xi, t) \quad (10)$$

where $\mathbf{w}(t)$ is the vector of the specific reaction rates w_i of the macroscopic bioreactions and φ is the vector of reaction rates.

2.2. Computation of the elementary flux modes and of minimal flux decomposition

2.2.1. Problem statement

A well known issue related to the EFMs representation is that the number of such vectors grows exponentially with the size of the network. This means that for detailed metabolic networks, such as the one considered in the following of this study, the computation of matrix \mathbf{E} becomes prohibitive.

In general, the decomposition of a flux distribution \mathbf{v} in the convex basis of elementary flux vectors \mathbf{e}_i does not necessitate the whole enumeration of the convex basis but requires only the knowledge of a few elementary vectors. Thus, the objective is to determine a minimal such decomposition (which directly complies with the target of a macroscopic model). Nonetheless, when the vector \mathbf{v} is the solution of an underdetermined metabolic

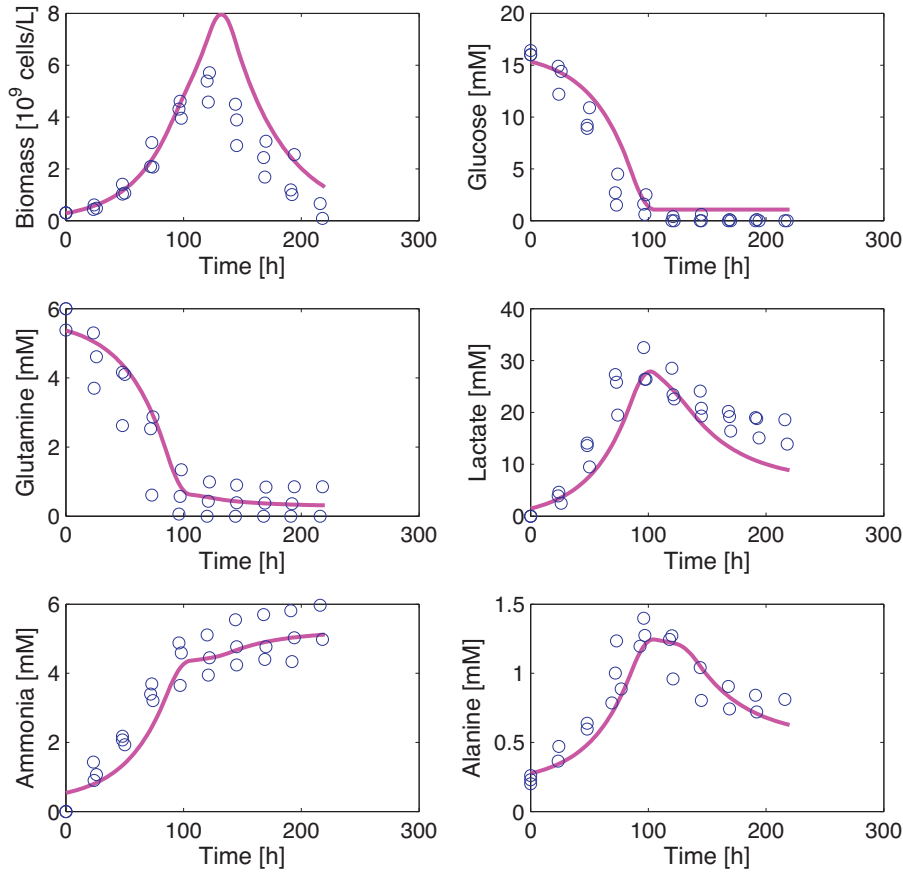


Fig. 6. Global model validation using a smaller glucose uptake rate.

flux analysis problem, the situation is more complex, though it may be possible to find a decomposition with even less elementary flux modes. Indeed, it is not known a priori which vector, among all admissible flux distributions, is the one that can be decomposed in the minimal number of elementary flux modes. The information needed for computing these elementary vectors can be obtained directly from the stoichiometric matrix \mathbf{N} together with the extracellular measurements. Herein, this methodology is used to compute this decomposition without actually evaluating the whole convex basis, thanks to the convex programming techniques presented in Jungers et al. (2011).

2.2.2. Definition of some polytopes of interest

If we consider system (3) and take the constraints imposed by the extracellular measurements into account, it is possible to write

$$\begin{pmatrix} \mathbf{N} \\ \mathbf{N}_m \end{pmatrix} \mathbf{v} = \begin{pmatrix} \mathbf{0} \\ \mathbf{v}_m \end{pmatrix} \quad \mathbf{v} \geq \mathbf{0}. \quad (11)$$

For a given metabolic network and a given set of measurements. \mathbf{N}_m stands for the stoichiometric matrix of the extracellular species and \mathbf{v}_m is the vector of measurements.

As demonstrated in Jungers et al. (2011) and Provost (2006), any admissible flux distribution \mathbf{v} can be expressed as a convex combination of $n-m$ elementary flux vectors \mathbf{e}_i . $n-m$ corresponds to the degrees of freedom of the system, if \mathbf{N} and \mathbf{N}_m are full rank matrices. Notice that the decomposition of \mathbf{v} in the convex basis $\{\mathbf{e}_i\}$ is not unique.

Moreover, if the number of measurements p is smaller than $n-m$, then there is at least one vector \mathbf{v}^* that can be expressed as a convex combination of only p elementary flux vectors. Hence,

the objective is to determine such a decomposition in a minimal number of elementary flux vectors $\{\mathbf{e}_i\}$.

Using Eq. (5), system (11) is equivalent to the system:

$$\begin{pmatrix} \mathbf{N}\mathbf{E} \\ \mathbf{N}_m\mathbf{E} \end{pmatrix} \mathbf{w} = \begin{pmatrix} \mathbf{0} \\ \mathbf{v}_m \end{pmatrix} \quad \mathbf{w} \geq \mathbf{0}. \quad (12)$$

We observe that the first equation $\mathbf{N}\mathbf{E}\mathbf{w} = \mathbf{0}$ is trivially satisfied independently of \mathbf{w} since by definition $\mathbf{N}\mathbf{E} = \mathbf{0}$. Hence, system (12) may be reduced to the second equation:

$$\mathbf{N}_m\mathbf{E}\mathbf{w} = \mathbf{v}_m \quad \mathbf{w} \geq \mathbf{0}. \quad (13)$$

or equivalently written

$$\begin{pmatrix} \mathbf{N}_m\mathbf{E} & -\mathbf{v}_m \end{pmatrix} \begin{pmatrix} \mathbf{w} \\ 1 \end{pmatrix} = 0. \quad (14)$$

In this form, it is clear that the set of admissible weighting vectors \mathbf{w} that satisfy Eq. (13) constitutes a convex polytope that will be denoted \mathcal{H} . Therefore, there exists a set of appropriate edge vectors \mathbf{h}_i such that any arbitrary convex combination of the form:

$$\mathbf{w} = \sum_i \beta_i \mathbf{h}_i \quad \beta_i \geq 0 \quad \sum_i \beta_i = 1 \quad (15)$$

is necessarily an admissible \mathbf{w} satisfying Eq. (13). The convex basis vectors \mathbf{h}_i have a critical property: the number of non-zero entries in these vectors is equal to the number of measurements p .

From a metabolic viewpoint, each vector \mathbf{h}_i is a solution \mathbf{w} of Eq. (13). Vectors $\mathbf{E}\mathbf{h}_i$ correspond to *minimal flux distributions* \mathbf{v} :

$$\hat{\mathbf{v}}_i = \mathbf{E}\mathbf{h}_i \quad \mathbf{v} \in \mathcal{F}. \quad (16)$$

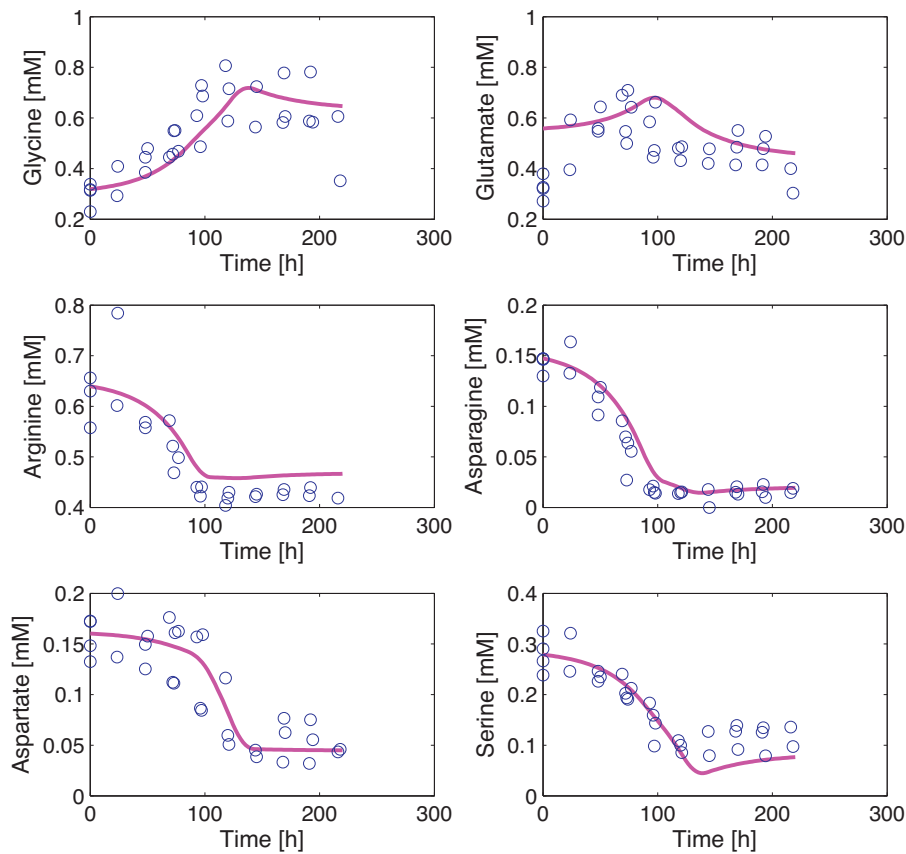


Fig. 7. Global model validation using a smaller glucose uptake rate.

Each minimal flux distribution \hat{v}_i represents the simplest pathways that satisfies the pseudo-steady state assumption and the constraints imposed by the extracellular measurements. Eq. (16) implies that a minimal flux distribution (in terms of EFMs) can be obtained by different combinations of EFMs and in turn, of metabolic pathways. This will be illustrated further in the article, when we will assess the calculation procedure of the minimal set of EFMs.

2.2.3. Decomposing \mathbf{v} in a convex basis

As already stated, the number of distinct extreme rays or cone vertices that are generated when computing the cone S may become very large because it combinatorially increases with the size of the underlying metabolic network. It is also the case for the number of vectors \mathbf{h}_i that are vertices of the polytope \mathcal{H} .

We apply here the method presented in Jungers et al. (2011) to decompose a flux distribution \mathbf{v} in a minimal number ($p < n - m$) of elementary flux modes. To this end, we introduce yet another cone $\mathcal{K} \subset \mathbb{R}^p$. This cone is the projection of S by the matrix \mathbf{N}_m : $\mathcal{K} = \{\mathbf{y} = \mathbf{N}_m \mathbf{v} : \mathbf{v} \geq \mathbf{0}, \mathbf{N} \mathbf{v} = \mathbf{0}\}$.

We know that the vector \mathbf{v}_m is in \mathcal{K} because of Eq. (11). So, \mathbf{v}_m can be expressed as a convex combination of p extreme rays y_i of cone \mathcal{K} (because \mathcal{K} has dimension p).

$$\mathbf{v}_m = \sum_i^p \alpha_i y_i \quad \alpha_i \geq 0 \quad \sum_i \alpha_i = 1. \quad (17)$$

Now, the extreme rays of \mathcal{K} are the projections of extreme rays \mathbf{e}_i of S under the matrix \mathbf{N}_m . This implies that the corresponding convex combination of the \mathbf{e}_i gives us the required \mathbf{v} . In other words, if y_i

is an extreme ray of the projected cone \mathcal{K} , then \mathbf{e}_i is an extreme ray of cone S .

$$\mathbf{v}_m = \mathbf{N}_m \mathbf{v} \Rightarrow y_i = \mathbf{N}_m \mathbf{e}_i \quad (18)$$

As \mathbf{v}_m has been decomposed in p extreme rays in Eq. (17), a decomposition in the extreme rays of cone S is also achieved

$$\mathbf{v}_m = \sum_1^p \alpha_i \mathbf{N}_m \mathbf{e}_i = \mathbf{N}_m \sum_1^p \alpha_i \mathbf{e}_i \quad (19)$$

and thus, \mathbf{v} is decomposed in a minimal set of p elementary flux vectors.

$$\mathbf{v} = \sum_1^p \alpha_i \mathbf{e}_i \quad (20)$$

For more details on the algorithm and the theory behind it, the reader is referred to references Jungers et al. (2009, 2011).

3. Results and discussion

3.1. Macroscopic bioreactions for cultures of CHO cells

In this section we apply the methodology described above to three detailed (and underdetermined) metabolic networks describing the metabolism of CHO-320 cells. Each network represents the metabolism of one of the culture phases of a cell in a batch culture: exponential growth, transition and death. For each of these networks, a minimal set of elementary flux modes is computed by applying the procedure described in Section 2.2. For reasons of space, the details of matrices \mathbf{N} for the growth, transition and death phases are not presented. To retrieve the list of reactions describing

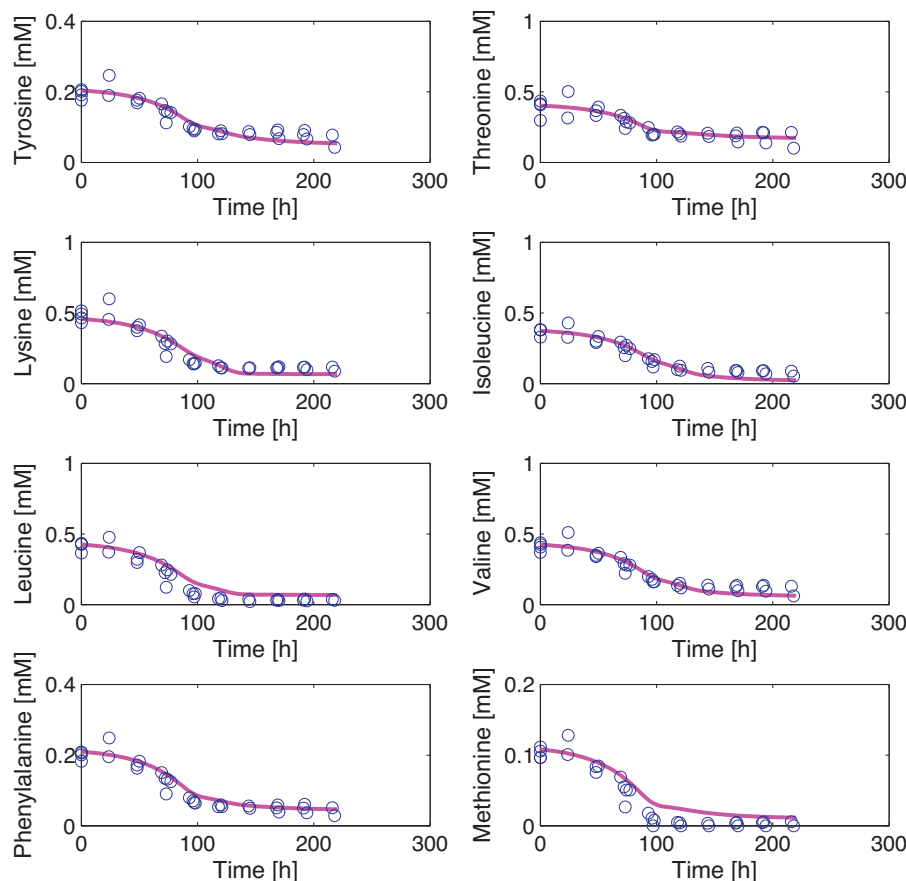


Fig. 8. Global model validation using a smaller glucose uptake rate.

the different phases, the reader is referred to references Zamorano et al. (2010) and Zamorano (2012). Their dimensions are (72×100) , (72×100) and (40×64) , respectively.

To apply this procedure we need to define stoichiometric matrices \mathbf{N} and \mathbf{N}_m and the vector of extracellular measurements \mathbf{v}_m for each phase. The set of experimental data contains, respectively 19, 18 and 17 extracellular measurements for the exponential growth, transition and death phases. The data set contains the time evolution of the extracellular concentration of the main substrates: glucose and glutamine, the main metabolic products: lactate, alanine and ammonia, and the concentration of 14 additional amino acids. The extracellular concentration of these species was determined through enzymatic kits and HPLC. The specific uptake and excretion rates are obtained by linear regression. These vectors of specific uptake/excretion rates \mathbf{v}_m are listed in Table 1.

The dimension of the vector \mathbf{v}_m will then determine the dimension of the matrix containing the minimal set of vectors \mathbf{e}_i (\mathbf{E}_{\min}). Each elementary vector defines a metabolic path linking extracellular substrates to final products, which can be translated into a macroscopic reaction. Proceeding in this way, the set of 19 macroscopic reactions presented in Table 2 describes the main metabolic processes occurring during the growth phase.

Thus, the minimal set of EFMs obtained for the exponential growth phase has been translated into a set of macroscopic bioreactions, from which a general model can be deduced. At this point, it is worth noticing that each run of the model reduction algorithm will yield different minimal sets of EFMs, thus giving different sets of macroscopic reactions. The reader is reminded about vectors \mathbf{h}_i and Eq. (16) which states that the pseudo-steady state assumption and the constraints imposed by the extracellular measurements can be satisfied by different minimal flux distributions $\hat{\mathbf{v}}_i$. Hence, each

time the calculation procedure is launched, a particular vector \mathbf{h}_i is found and in turn, a minimal flux distribution $\hat{\mathbf{v}}_i$. An estimation of the reaction rates for the macroreactions are obtained from Eq. (13). As $\mathbf{N}_m \mathbf{E}$ is a $p \times p$ matrix, then \mathbf{w} is easily obtained from:

$$\mathbf{w} = (\mathbf{N}_m \mathbf{E})^{-1} \mathbf{v}_m \quad (21)$$

The resulting reaction rates w_i for each of the macroscopic reactions taking place during the exponential growth phase are listed in Table 3.

In the same way, a minimal set of elementary vectors for the transition phase is obtained. The number of extreme rays \mathbf{e}_i matches the number of entries in vector \mathbf{v}_m . Thus, the 18 resulting elementary flux vectors are presented in Table 4, from which a set of macroscopic reactions is defined. Notice that the metabolic changes corresponding to this phase of the culture are reflected by the macroscopic reactions obtained. Lactate, alanine and glutamate are now consumed as substrates, and since glucose is depleted, it no longer appears as a substrate. The estimated reaction rates w_i are listed in Table 3.

The same procedure is now applied to the reaction network defining the metabolism of the death phase of the culture. As vector \mathbf{v}_m includes 17 experimental measurements, the same number of elementary vectors are obtained. This set of extreme rays generate the corresponding macroscopic bioreactions presented in Table 5. Now that cells are dying, there is no production of biomass any longer and the metabolism is centered in the production of energy with CO_2 as main product. The resulting reaction rates w_i are presented in Table 3.

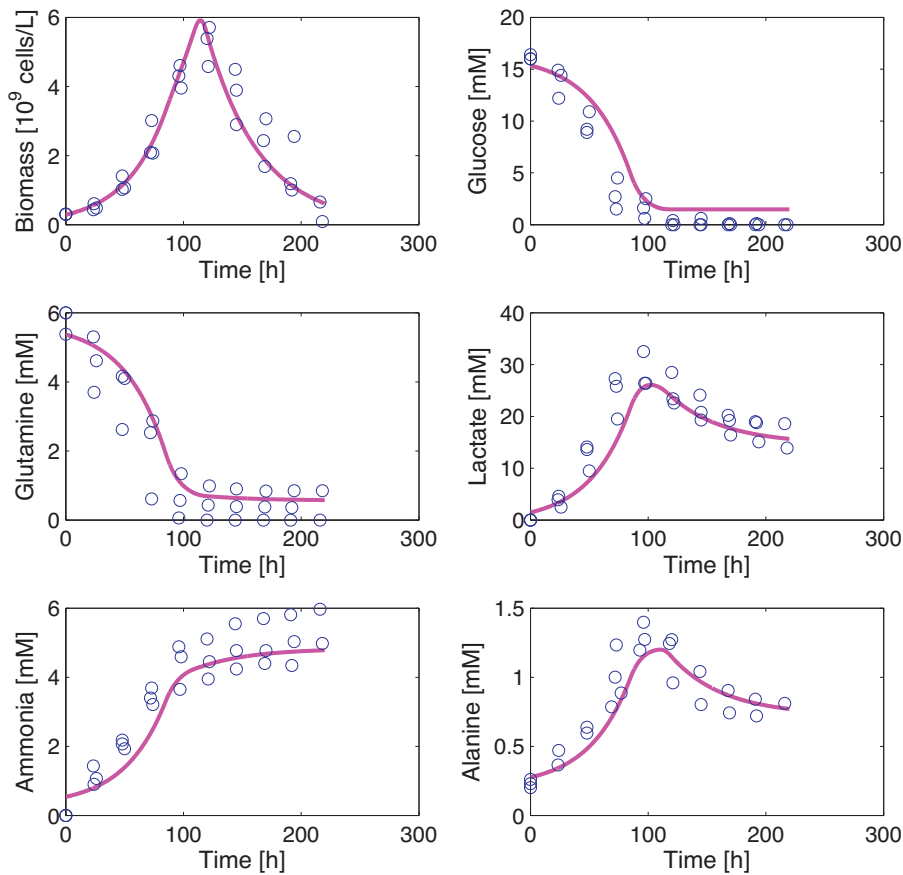


Fig. 9. Global model validation using a smaller glucose uptake rate and physiological switching functions.

Table 1
Specific uptake/excretion rates for the three cell culture phases.

Specie	Exponential growth phase	Transition phase	Death phase
Glucose	$-1.6383 \pm 0.244e^{-1}$	–	–
Glutamine	$-4.7922 \pm 1.107e^{-2}$	$-1.4582 \pm 7.678e^{-3}$	$-8.9527 \pm 62.97e^{-4}$
Arginine	$-1.7381 \pm 1.659e^{-3}$	$-8.9108 \pm 0.271e^{-5}$	$5.1413 \pm 16.66e^{-5}$
Asparagine	$-1.2354 \pm 0.203e^{-3}$	$-1.7873 \pm 3.316e^{-5}$	$6.0603 \pm 10.76e^{-5}$
Aspartate	$-2.7112 \pm 4.304e^{-4}$	$-4.6172 \pm 4.601e^{-4}$	$-7.4483 \pm 20.77e^{-5}$
Isoleucine	$-1.7422 \pm 0.521e^{-3}$	$-4.1392 \pm 2.982e^{-4}$	$-1.7901 \pm 2.393e^{-4}$
Leucine	$-2.9556 \pm 0.610e^{-3}$	$-3.1471 \pm 2.109e^{-4}$	$-1.1150 \pm 8.286e^{-5}$
Lysine	$-3.0675 \pm 0.839e^{-3}$	$-2.7181 \pm 1.628e^{-4}$	$-4.9260 \pm 17.34e^{-5}$
Methionine	$-8.1777 \pm 1.777e^{-4}$	$-6.6621 \pm 6.668e^{-5}$	–
Phenylalanine	$-1.1747 \pm 0.309e^{-3}$	$-1.0902 \pm 0.832e^{-4}$	$-4.6531 \pm 18.38e^{-5}$
Serine	$-1.0054 \pm 0.499e^{-3}$	$-4.4716 \pm 3.295e^{-4}$	$1.5091 \pm 4.229e^{-4}$
Threonine	$-1.5358 \pm 0.928e^{-3}$	$-1.2195 \pm 2.679e^{-4}$	$-1.2157 \pm 7.073e^{-4}$
Tyrosine	$-8.7011 \pm 3.171e^{-4}$	$-8.5351 \pm 7.158e^{-5}$	$-1.2778 \pm 2.528e^{-4}$
Valine	$-2.0238 \pm 0.664e^{-3}$	$-2.7412 \pm 2.827e^{-4}$	$-1.5805 \pm 4.369e^{-4}$
Lactate	$2.9880 \pm 0.599e^{-1}$	$-2.0169 \pm 4.971e^{-2}$	$-3.8359 \pm 3.793e^{-2}$
NH ₄ ⁺	$3.8858 \pm 0.954e^{-2}$	$1.4428 \pm 8.118e^{-3}$	$1.5064 \pm 10.11e^{-3}$
Glycine	$2.6166 \pm 0.847e^{-3}$	$4.6293 \pm 14.47e^{-4}$	$-5.3266 \pm 22.34e^{-4}$
Alanine	$1.0273 \pm 0.144e^{-2}$	$-1.1855 \pm 56.37e^{-4}$	$-2.1682 \pm 1.527e^{-3}$
Glutamate	$3.0143 \pm 1.942e^{-3}$	$-9.7355 \pm 8.015e^{-4}$	$-9.0875 \pm 11.29e^{-4}$

3.2. A piecewise dynamic model of CHO-320 cells

An estimation of the maximum reaction rates has been obtained for each of the cell culture phase (see Table 3). To take account of possible substrate limitations, and guarantee concentration positivity during model simulation, it is suggested to modulate these maximum rates with Monod factors.

$$r_i = w_i \frac{S_1}{(k_{s1} + S_1)} \frac{S_2}{(k_{s2} + S_2)} \dots \frac{S_{n_i}}{(k_{s_{n_i}} + S_{n_i})}. \quad (22)$$

Subindex n_i indicates the number of substrates participating in reaction i .

Thus, the dynamical model can be rewritten as:

$$\frac{d\xi}{dt} = \mathbf{K}rX. \quad (23)$$

In order to complete the model, it is necessary to select numerical values for the half-saturation constants of substrates. Our aim in this study is to propose a model structure and not to estimate these values from experimental data. Clearly, our database is insufficient for this latter purpose. Here, we select somewhat arbitrary values

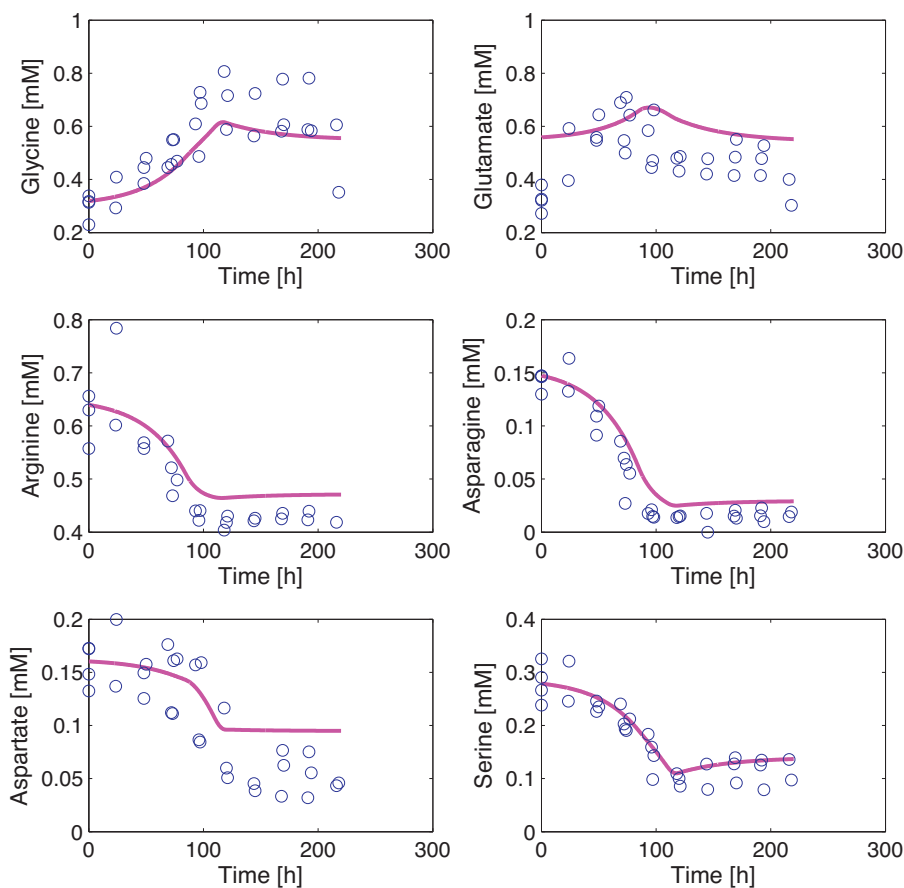


Fig. 10. Global model validation using a smaller glucose uptake rate and physiological switching functions.

Table 2
Macroscopic reactions for the exponential growth phase.

EFM	Macroscopic reaction
e_1	$\text{Tyr} \rightarrow \text{Glu} + 4 \text{CO}_2$
e_2	$\text{Glucose} + 1.7 \text{Gln} \rightarrow 1.7 \text{Lactate} + 3.3 \text{NH}_4^+ + 6 \text{CO}_2$
e_3	$\text{Gln} \rightarrow \text{Glu} + \text{NH}_4^+$
e_4	$\text{Ser} \rightarrow \text{Gly}$
e_5	$\text{Asn} \rightarrow \text{Lactate} + \text{Urea}$
e_6	$3.3 \text{Glucose} + 6.4 \text{Gln} + \text{Asn} + 1.9 \text{Asp} + 1.2 \text{Arg} + 1.4 \text{Thr} + 1.7 \text{Lys} + 1.6 \text{Val} + 1.3 \text{Ile} + 6.5 \text{Leu} + 1.7 \text{Phe} + \text{Met} + 1.2 \text{Pro} + 0.3 \text{Trp} + 0.5 \text{His} + 0.2 \text{Eth} + 0.4 \text{Cho} \rightarrow 25.8 \text{Biomass} + 2.9 \text{Ala} + 5 \text{NH}_4^+ + 13.1 \text{CO}_2$
e_7	$15.2 \text{Glucose} + 7.7 \text{Gln} + 4.7 \text{Asn} + 14.2 \text{Arg} + 6.5 \text{Thr} + 13.5 \text{Lys} + 7.2 \text{Val} + 5.8 \text{Ile} + 10 \text{Leu} + 7.8 \text{Phe} + 4.6 \text{Met} + 5.7 \text{Pro} + 25.9 \text{Trp} + 2.5 \text{His} + 0.7 \text{Eth} + 2 \text{Cho} \rightarrow 118.6 \text{Biomass} + 15.8 \text{Ala} + 8.6 \text{Urea} + \text{NH}_4^+ + 134.2 \text{CO}_2$
e_8	$\text{Glucose} + 1.7 \text{Val} \rightarrow 3.3 \text{Lactate} + 1.7 \text{NH}_4^+ + 4.3 \text{CO}_2$
e_9	$2.1 \text{Glucose} + 2.5 \text{Gln} + \text{Asn} + 1.2 \text{Arg} + 3.4 \text{Thr} + 1.5 \text{Lys} + 1.6 \text{Val} + 4.2 \text{Ile} + 5.1 \text{Leu} + 1.7 \text{Phe} + 1 \text{Met} + 1.2 \text{Pro} + 0.3 \text{Trp} + 0.5 \text{His} + 0.2 \text{Eth} + 0.4 \text{Cho} \rightarrow 25.8 \text{Biomass} + \text{NH}_4^+ + 4.7 \text{CO}_2$
e_{10}	$15.2 \text{Glucose} + 7.7 \text{Gln} + 4.7 \text{Asn} + 9.4 \text{Arg} + 6.5 \text{Thr} + 6.5 \text{Lys} + 7.2 \text{Val} + 68.7 \text{Ile} + 10 \text{Leu} + 7.8 \text{Phe} + 4.6 \text{Met} + 5.7 \text{Pro} + 1.5 \text{Trp} + 2.5 \text{His} + 0.7 \text{Eth} + 2 \text{Cho} \rightarrow 118.6 \text{Biomass} + 19 \text{Lactate} + 30.6 \text{Ala} + 3.8 \text{Urea} + \text{NH}_4^+ + 75.9 \text{CO}_2$
e_{11}	$\text{Gln} \rightarrow \text{Ala} + \text{NH}_4^+ + 2 \text{CO}_2$
e_{12}	$6.6 \text{Glucose} + 2.4 \text{Gln} + \text{Asn} + 1.2 \text{Arg} + 1.4 \text{Thr} + 8.1 \text{Lys} + 1.5 \text{Val} + 1.2 \text{Ile} + 2.1 \text{Leu} + 1.7 \text{Phe} + 2.4 \text{Met} + 1.2 \text{Pro} + 0.3 \text{Trp} + 0.5 \text{His} + 0.1 \text{Eth} + 0.4 \text{Cho} \rightarrow 25.2 \text{Biomass} + 4.3 \text{Gly} + 3.9 \text{NH}_4^+ + 21 \text{CO}_2$
e_{13}	$\text{Gln} \rightarrow \text{Lactate} + \text{Urea} + \text{CO}_2$
e_{14}	$\text{Glucose} \rightarrow 1.7 \text{Lactate} + \text{CO}_2$
e_{15}	$6.8 \text{Glucose} + 1.7 \text{Gln} + \text{Asn} + 6.2 \text{Arg} + 1.4 \text{Thr} + 1.4 \text{Lys} + 1.6 \text{Val} + 1.3 \text{Ile} + 6.7 \text{Leu} + 1.7 \text{Phe} + \text{Met} + 1.2 \text{Pro} + 0.3 \text{Trp} + 0.5 \text{His} + 0.2 \text{Eth} + 0.4 \text{Cho} \rightarrow 25.8 \text{Biomass} + 7 \text{Lactate} + 4.9 \text{Urea} + 6 \text{NH}_4^+ + 14.5 \text{CO}_2$
e_{16}	$49.6 \text{Glucose} + 7.7 \text{Gln} + 4.7 \text{Asn} + 22.7 \text{Arg} + 6.5 \text{Thr} + 37.9 \text{Lys} + 7.2 \text{Val} + 5.8 \text{Ile} + 10 \text{Leu} + 7.8 \text{Phe} + 4.6 \text{Met} + 5.7 \text{Pro} + 1.5 \text{Trp} + 2.5 \text{His} + 0.7 \text{Eth} + 2 \text{Cho} \rightarrow 118.6 \text{Biomass} + 57.3 \text{Gly} + 17.1 \text{Urea} + \text{NH}_4^+ + 136.9 \text{CO}_2$
e_{17}	$1.2 \text{Glucose} + \text{Arg} \rightarrow 3 \text{Lactate} + \text{Urea} + 2 \text{NH}_4^+ + 3.2 \text{CO}_2$
e_{18}	$7.3 \text{Glucose} + 3.5 \text{Gln} + \text{Asn} + 1.2 \text{Arg} + 1.4 \text{Thr} + 8.1 \text{Lys} + 1.5 \text{Val} + 1.2 \text{Ile} + 2.1 \text{Leu} + 1.7 \text{Phe} + \text{Met} + 1.2 \text{Pro} + 0.3 \text{Trp} + 0.5 \text{His} + 0.1 \text{Eth} + 0.4 \text{Cho} \rightarrow 25.2 \text{Biomass} + 4.9 \text{Lactate} + 8.7 \text{NH}_4^+ + 22.2 \text{CO}_2$
e_{19}	$\text{Glucose} + 1.7 \text{Gln} \rightarrow 3.3 \text{Lactate} + 3.3 \text{NH}_4^+ + 4.3 \text{CO}_2$

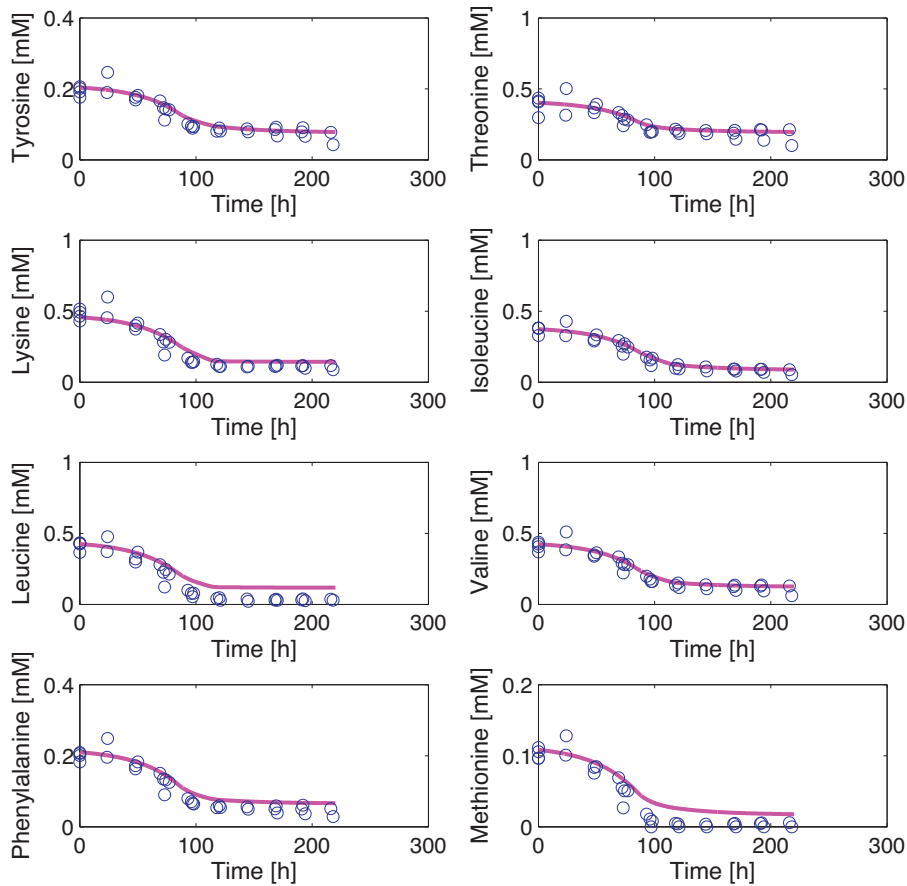


Fig. 11. Global model validation using a smaller glucose uptake rate and physiological switching functions.

equal to 0.1 mM, i.e., values small enough to not interfere during the growth phase but large enough to avoid stiffness difficulties in the simulation of the model differential equations. The same idea has been used in Provost and Bastin (2004).

Consequently, a local dynamic model is obtained for each of the cell culture phases. In Figs. 1 and 2 the prediction of the three different models is presented. As expected, all three models fit well the available data in their respective time span.

A global model describing the complete dynamics of a CHO-320 cell culture, can be defined as an interpolation between the three models obtained in the previous section for growth, transition and

death phases. The influence of each model is controlled by means of weighting functions ϕ_g , ϕ_m and ϕ_d (see Murray-Smith and Johansen (1997) for more on the multi-model approach), such that the global model is formulated as follows:

$$\frac{d\xi}{dt} = \phi_g \frac{d\xi_g}{dt} + \phi_m \frac{d\xi_m}{dt} + \phi_d \frac{d\xi_d}{dt}. \tag{24}$$

Many local basis functions could be used. One of the simplest option is provided by linear functions of time ϕ_g , ϕ_m and ϕ_d , as shown in Fig. 3. In order to blend the three models, the first transition occurs in a time span starting from 75 h until 95 h, time of the culture at

Table 3
Reaction rates for the three sets of macroscopic reactions.

Reaction rate	Exponential growth phase	Transition phase	Death phase
w ₁	7.6104e ⁻⁴	1.4006e ⁻⁴	1.9790e ⁻⁵
w ₂	3.3737e ⁻³	3.8043e ⁻⁴	1.9790e ⁻⁵
w ₃	1.9371e ⁻⁴	4.1514e ⁻⁵	5.8637e ⁻⁶
w ₄	9.2342e ⁻⁴	5.7292e ⁻⁴	2.0670e ⁻⁴
w ₅	5.2333e ⁻⁴	8.3348e ⁻⁷	9.2354e ⁻⁵
w ₆	1.7039e ⁻⁴	5.1261e ⁻⁵	2.4921e ⁻⁵
w ₇	7.8766e ⁻⁶	2.9480e ⁻⁴	1.1288e ⁻⁴
w ₈	6.1698e ⁻⁴	3.2716e ⁻⁴	3.6726e ⁻²
w ₉	1.8203e ⁻⁴	3.3813e ⁻²	5.9150e ⁻⁴
w ₁₀	4.0478e ⁻⁶	2.7660e ⁻⁴	6.2670e ⁻⁵
w ₁₁	8.0719e ⁻³	5.4907e ⁻⁵	7.6960e ⁻⁵
w ₁₂	9.4097e ⁻⁵	5.6892e ⁻⁴	7.3303e ⁻⁷
w ₁₃	2.3533e ⁻²	2.6781e ⁻⁴	2.4188e ⁻⁵
w ₁₄	1.7277e ⁻¹	2.7978e ⁻⁵	2.1403e ⁻⁴
w ₁₅	1.0689e ⁻⁵	2.4642e ⁻⁵	7.2050e ⁻⁴
w ₁₆	1.5793e ⁻⁵	5.4348e ⁻⁵	7.4763e ⁻⁵
w ₁₇	1.0180e ⁻³	7.0945e ⁻⁵	3.3575e ⁻⁴
w ₁₈	8.1690e ⁻⁶	9.0659e ⁻⁵	-
w ₁₉	6.4727e ⁻³	-	-

Table 4
Macroscopic reactions for the transition phase.

EFM	Macroscopic reaction
e_1	$\text{Tyr} \rightarrow \text{NH}_4^+ + 9 \text{CO}_2$
e_2	$\text{Gln} \rightarrow 2 \text{NH}_4^+ + 3 \text{CO}_2$
e_3	$3 \text{Leu} + \text{Met} \rightarrow 2 \text{Urea} + 20 \text{CO}_2$
e_4	$\text{Ser} \rightarrow \text{Gly}$
e_5	$\text{Asn} \rightarrow \text{Urea} + 3 \text{CO}_2$
e_6	$13.7 \text{Lactate} + 2.2 \text{Gln} + \text{Asn} + 2.6 \text{Asp} + 1.2 \text{Arg} + 1.4 \text{Thr} + 1.4 \text{Lys} + 1.6 \text{Val} + 1.3 \text{Ile}$ $+ 2.2 \text{Leu} + 1.7 \text{Phe} + \text{Met} + 1.9 \text{Ala} + 4.5 \text{Glu} + 1.2 \text{Pro} + 0.3 \text{Trp} + 0.5 \text{His} + 0.2 \text{Etn} + 0.4 \text{Cho}$ $\rightarrow 25.8 \text{Biomass} + 0.7 \text{Urea} + 23.8 \text{CO}_2$
e_7	$\text{Ala} + \text{Asp} \rightarrow \text{Urea} + 4 \text{CO}_2$
e_8	$\text{Val} \rightarrow \text{Gly} + 2 \text{CO}_2$
e_9	$\text{Lactate} \rightarrow 3 \text{CO}_2$
e_{10}	$\text{Ile} + \text{Leu} \rightarrow \text{Urea} + 9 \text{CO}_2$
e_{11}	$\text{Lys} + 2 \text{Phe} \rightarrow 2 \text{Urea} + 18 \text{CO}_2$
e_{12}	$\text{Gln} \rightarrow \text{Urea} + 4 \text{CO}_2$
e_{13}	$\text{Lys} + 2 \text{Glu} \rightarrow 2 \text{Urea} + 10 \text{CO}_2$
e_{14}	$\text{Lys} + 2 \text{Val} \rightarrow 2 \text{Urea} + 10 \text{CO}_2$
e_{15}	$\text{Thr} + \text{Ile} \rightarrow \text{Urea} + 9 \text{CO}_2$
e_{16}	$\text{Thr} + 1.5 \text{Lys} \rightarrow 2 \text{Urea} + 9 \text{CO}_2$
e_{17}	$2 \text{Asp} + \text{Lys} \rightarrow 2 \text{Urea} + 8 \text{CO}_2$
e_{18}	$\text{Lys} + 2 \text{Ile} \rightarrow 2 \text{Urea} + 12 \text{CO}_2$

which glucose is depleted. The second transition starts at $t = 123$ h and finishes at $t = 143$ h, a time range where some kind of stress in the culture medium triggers cellular apoptosis or programmed cell death. The time selection for the first model transition is derived from the fact that the last measurement points of the growth phase occurs at 72–74 h and the first measurement points of the transition phase are at 96–98 h. In the same way, the time selection for the second transition comes from the last measurement points of the transition phase and the first points of the death phase, at 120–122 h and 144–145 h, respectively. The simulation results are presented in Figs. 4 and 5.

While the model reproduces quite well the evolution of cellular density and main substrates and products, it fails to provide good results for all metabolites. Indeed, at the end of the growth phase, the model stops predicting the consumption of certain amino acids such as arginine, asparagine, threonine, leucine, isoleucine, valine, phenylalanine and methionine. Hence, the transition phase model starts with wrong initial concentrations and is not able to catch up with the real data. To alleviate the problem of the erroneous model prediction for certain amino acids, we search for those macroscopic reactions where these amino acids participate. It appears that all nine amino acids participate in almost exactly the same reactions. In addition, in all these reactions glucose appears as a substrate. The kinetic expressions of the reaction rates r are modeled by Monod kinetics and thus, they depend on glucose concentration as a multiplication factor. Consequently, the concentration of these amino acids do not vary any longer, as the glucose concentration depletes.

Clearly, the early disappearance of glucose from the medium is the cause of this problem. The exponential growth phase model presented in Table 2 has been determined from the experimental measurements collected between 0 and 80 h. Due to the reduced number of measurement points, the error in the determination of the specific uptake rate of glucose (and all other species) might be significant. Indeed, a smaller consumption rate of glucose would maybe yield a macroscopic model capable of a better fit for the amino acids in question. Thus, we selected from Table 1 a smaller specific uptake rate of glucose within the confidence interval of the estimated value, so as to compute a new minimal set of EFMs, and in turn, a new model for the exponential growth phase. The set of macroscopic reactions obtained along with their corresponding reaction rates w_i are presented in Table 6.

The global model is constructed as before using linear functions of time. Now, the first transition starts at $t = 85$ h until $t = 100$ h. In this way, the overlapping of the exponential growth and transition

phase models occurs later, allowing the first to have an influence on the global model for a longer time. The time span of the second transition remains identical, starting at $t = 123$ h and finishing at $t = 143$ h. The simulation results are presented in Figs. 6–8.

3.2.1. Physiological switching functions

Clearly, a model based on time weighting functions has no physiological interpretation and thus, it is desirable to develop a model capable of reproducing the shift from one culture phase to the next based on the evolution of some metabolite concentrations. For this purpose, a global model is now established using linear functions of metabolic dependent variables. It is known that the exponential growth phase ends once the glucose concentration in the culture medium decreases below a critical level to allow rapid cellular division. At this moment, the produced lactate is consumed as the carbon source instead of glucose. Accordingly, the first switching function has been selected in dependence of the ratio between the glucose concentration (G) and the cellular density (X) at each time instant. Normally, in a batch culture this G/X ratio will decrease as the glucose is consumed to produce biomass. On the other hand, cellular death can be triggered by a number of environmental factors such as hypoxia, waste by-product accumulation, mechanical agitation and nutrient depletion among others (Arden and Betenbaugh, 2004; Laken and Leonard, 2001). Based on the limited information provided by the evolution of the

Table 5
Macroscopic reactions for the death phase.

EFM	Macroscopic reaction
e_1	$\text{Ala} + \text{Gly} \rightarrow \text{Asn}$
e_2	$\text{Lys} + 2 \text{Gly} \rightarrow 2 \text{Urea} + 6 \text{CO}_2$
e_3	$\text{Asp} + 3 \text{Leu} + \text{Pro} \rightarrow \text{Ser} + \text{Arg} + 18 \text{CO}_2$
e_4	$\text{Gly} \rightarrow \text{NH}_4^+ + \text{CO}_2$
e_5	$\text{Thr} \rightarrow \text{NH}_4^+ + 3 \text{CO}_2$
e_6	$3 \text{Ala} + 1 \text{Pro} \rightarrow \text{Arg} + 8 \text{CO}_2$
e_7	$\text{Glu} \rightarrow \text{Ser} + 2 \text{CO}_2$
e_8	$\text{Lactate} \rightarrow 3 \text{CO}_2$
e_9	$\text{Gln} \rightarrow 2 \text{NH}_4^+ + 5 \text{CO}_2$
e_{10}	$2 \text{Val} \rightarrow \text{Urea} + 9 \text{CO}_2$
e_{11}	$2 \text{Ile} \rightarrow \text{Urea} + 11 \text{CO}_2$
e_{12}	$\text{Asp} + \text{Glu} \rightarrow \text{Urea} + 8 \text{CO}_2$
e_{13}	$2 \text{Phe} \rightarrow \text{Urea} + 17 \text{CO}_2$
e_{14}	$\text{Glu} \rightarrow \text{NH}_4^+ + 5 \text{CO}_2$
e_{15}	$2 \text{Ala} \rightarrow \text{Urea} + 5 \text{CO}_2$
e_{16}	$\text{Tyr} \rightarrow \text{NH}_4^+ + 9 \text{CO}_2$
e_{17}	$\text{Ala} \rightarrow \text{NH}_4^+ + 3 \text{CO}_2$

Table 6
Macroscopic reactions for the exponential growth phase.

EFM	Macroscopic reaction	Reaction rate w
e_1	16.2 Glucose + 3.1 Gln + 1.9 Asn + 3.4 Asp + 2.2 Arg + 1.4 Tyr + 2.6 Thr + 15.4 Lys + 2.9 Val + 2.3 Ile + 4 Leu + 1.7 Phe + Met + 3.1 Pro + 0.6 Trp + His + 0.3 Eth + 0.8 Cho → 47.1 Biomass + 14.9 Gly + 43.6 CO ₂	$3.3637e^{-3}$
e_2	Lysine → 2 NH ₄ ⁺ + 6 CO ₂	$1.2885e^{-3}$
e_3	Val → Lactate + NH ₄ ⁺ + 2 CO ₂	$6.8944e^{-3}$
e_4	Gln → Lactate + 2 NH ₄ ⁺ + 2 CO ₂	$5.8354e^{-2}$
e_5	Glucose → 2 Lactate	$8.9550e^{-1}$
e_6	Ser + Arg → Ala + Glu + NH ₄ ⁺ + Urea	$2.6505e^{-4}$
e_7	Gln → Ala + NH ₄ ⁺ + 2 CO ₂	$3.2234e^{-3}$
e_8	Ile → Glu + CO ₂	$3.3120e^{-5}$
e_9	Glucose → 6 CO ₂	$1.5911e^{-2}$
e_{10}	Thr → Gly + 2 CO ₂	$6.4803e^{-5}$
e_{11}	Asn + Arg → 2 Ala + 2 Urea + 2 CO ₂	$2.6428e^{-4}$
e_{12}	Ser + 4 Arg + Met → 6 Ala + 6 Urea + 7 CO ₂	$2.1242e^{-5}$
e_{13}	Tyr + Thr → Urea + 11 CO ₂	$1.2274e^{-5}$
e_{14}	Ser + 4 Leu + Met → 2 Ala + 23 CO ₂	$2.8599e^{-4}$
e_{15}	Tyr → Ala + 6 CO ₂	$6.1860e^{-5}$
e_{16}	Ile → Ala + 3 CO ₂	$1.3218e^{-4}$
e_{17}	Gln → Urea + 4 CO ₂	$1.4200e^{-2}$
e_{18}	Phe → Ala + 6 CO ₂	$1.2058e^{-4}$
e_{19}	Ser + 2 Phe + Met → 2 Urea + 23 CO ₂	$4.9886e^{-6}$

extracellular measurements at hand, it could be assumed that the cellular death is caused by the accumulation of a certain toxic or inhibitory metabolite. Even though the concentration of ammonia at the last stage of the culture is not high enough so as to become toxic, the second switch has been selected as a function of the ammonia concentration at each time instant. In this way, the second transition occurs once the ammonia concentration reaches a critical level (selected as “toxic”), causing apoptosis.

To construct the global model, the first transition starts at $G/X=1.5$ until $G/X=0.2$ and the second starts when the ammonia concentration N reaches 4.25 mM and finishes when $N=4.35$ mM. The simulation results are presented in Figs. 9–11.

The global model using the selected switching functions is able to reproduce quite well the experimental data, which suggests the potential of these physiological variables to be used as switching functions in a piecewise model.

4. Conclusions

Dynamic modeling of animal cell cultures is a delicate task that has attracted considerable attention in the last decades, with models ranging from low-dimensional macroscopic models to complex models mixing knowledge about the metabolic network and kinetic models (Ahn and Antoniewicz, 2011).

In this study, a procedure for the derivation of macroscopic dynamic models from detailed metabolic networks is presented, and discussed based on an application example related to batch cultures of CHO-320 cells. In particular, the relatively high complexity of the metabolic network makes impossible the computation of the complete set of elementary flux modes due to combinatorial explosion. An alternative procedure is therefore applied, where an admissible flux distribution is decomposed into a minimal set of elementary flux modes, whose number is equal to the number of available extracellular measurements. Thus, the minimal set can be computed directly, without enumerating the full collection of EFMs. Model reduction based on this minimal decomposition provides sets of macroscopic bioreactions in a convenient way, as well as estimates of the maximum reaction rates. Dynamic models with suitable properties can be obtained through the introduction of classical Monod factors. Piecewise models for the different cell culture phases can also be easily constructed, using linear weighting functions (to switch from one culture phase

either in dependence on time, or on the evolution of extracellular concentrations.

To improve the model fit, it was necessary to adjust the glucose uptake rate within its confidence interval (as determined by a standard least-squares procedure). This might be due to a lack of data (i.e. uncertainty in the glucose uptake rate) or a slower assimilation of glucose (non steady-state effect).

Acknowledgments

This article presents research results of the Belgian Network DYSCO (Dynamical Systems, Control, and Optimization), funded by the Interuniversity Attraction Poles Programme, initiated by the Belgian State, Science Policy Office. The authors acknowledge the support of the FEDER 2007–2013 research program HAINAUT BIOMED, in the framework of the OCPAM project. R.M. Jungers is a F.R.S.-FNRS fellow. The scientific responsibility rests with its authors.

References

- Ahn, W.S., Antoniewicz, M.R., 2011. Review – towards dynamic metabolic flux analysis in CHO cell cultures. *Biotechnology Journal* 6, 1–14.
- Arden, N., Betenbaugh, M.J., 2004. Life and death in mammalian cell culture: strategies for apoptosis inhibition. *Trends in Biotechnology* 22, 174–180.
- Bastin, G., Dochain, D., 1990. On-line Estimation and Adaptive Control of Bioreactors. Bernard, O., Bastin, G., 2005. On the estimation of the pseudo-stoichiometric matrix for macroscopic mass balance modelling of biotechnological processes. *Mathematical Biosciences* 193, 51–77.
- Chen, L., Bastin, G., 1996. Structural identifiability of the yield coefficients in bioprocess models when the reaction rates are unknown. *Mathematical Biosciences* 132, 35–67.
- Haag, J.E., Wouwer, A.V., Bogaerts, P., 2005. Dynamic modeling of complex biological systems: a link between metabolic and macroscopic description. *Mathematical Biosciences* 193, 25–49.
- Hulhoven, X., Vande Wouwer, A., Bogaerts, P., 2005. On a systematic procedure for the predetermination of macroscopic reaction schemes. *Bioprocess Biosystem Engineering* 27 (5), 283–291.
- Jungers, R., Zamorano, F., Blondel, V., Wouwer, A.V., Bastin, G., 2009. A fast algorithm for computing a minimal decomposition of a metabolic flux vector in terms of elementary flux vectors. In: Vienna Conference on Mathematical Modelling – MATHMOD 2009.
- Jungers, R.M., Zamorano, F., Blondel, V., Wouwer, A.V., Bastin, G., 2011. Fast computation of minimal elementary decompositions of metabolic flux vectors. *Automatica* 47, 1255–1259.
- Laken, H., Leonard, M., 2001. Understanding and modulating apoptosis in industrial cell culture. *Current Opinion in Biotechnology* 12, 175–179.
- Mocquet, C., Bernard, O., Sciandra, A., 2010. Cell cycle modelling of microalgae grown under a light-dark signal. In: CAB 2010.

- Murray-Smith, R., Johansen, T.A., 1997. *Multiple Model Approaches to Modelling and Control*. Taylor and Francis, London.
- Provost, A., Bastin, G., 2004. Dynamic metabolic modelling under the balanced growth condition. *Journal of Process Control* 14, 717–728.
- Provost, A., Bastin, G., Schneider, Y.-J., June 2007. From metabolic networks to minimal dynamic bioreaction models. In: 10th International IFAC Symposium on Computer Applications in Biotechnology. IFAC.
- Provost, A., 2006. *Metabolic design of dynamic bioreaction models*. Ph.D. thesis, Université Catholique de Louvain.
- Smets, I., 2002. *Analysis and synthesis of mathematical algorithms for optimization and control of complex biochemical conversion processes*. Ph.D. thesis, Department of Chemical Engineering.
- Zamorano, F., Wouwer, A.V., Bastin, G., 2010. A detailed metabolic flux analysis of an underdetermined network of CHO cells. *Journal of Biotechnology* 150, 497–508.
- Zamorano, F., 2012. *Metabolic flux analysis of CHO cell cultures*. Ph.D. thesis, Université de Mons.